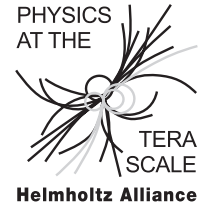


Helmholtz Alliance at the Terascale
Data Analysis Group
Introductory School on Terascale Physics
21 – 25 February, 2011



Tutorial on Top-Quark Physics

Introduction to the Tevatron, the CDF Detector and Top-Quark Physics

Dr. D. Hirschtühl and Prof. Dr. W. Wagner
Bergische Universität Wuppertal

In the tutorial on top-quark physics you will analyze proton-antiproton collision data recorded by the CDF detector at Fermilab. You will learn how to select an enriched sample to top-antitop quark candidate events and how to measure the top-quark mass using the so-called *template method*. In this introductory text we will provide you with some basic background information on the Tevatron accelerator, the CDF detector and on top-quark production in hadron collisions.

1 Introduction

The top quark was discovered by the CDF and $D\bar{0}$ collaborations in 1995 at the Tevatron proton antiproton collider and still remains one of the least well-studied elementary particles discovered so far. In particular, the measurement of its mass constrains the mass of the Higgs boson, the last particle to be discovered in the Standard Model.

This tutorial is concerned with the observation of top quarks and with the measurement of the top quark mass. The data used here have been collected from January 2002 until February 2006 by the CDF detector. In the Tevatron ring, intense beams of protons and antiprotons are accelerated, stored and finally collided within each of the two detectors. The center of mass energy of the proton antiproton collisions is $\sqrt{s} = 1.96$ TeV. Before the protons and antiprotons reach the Tevatron storage ring they pass through a long chain of accelerators which is displayed in Figure 1.

2 The CDF Detector

The CDF detector is a general purpose detector consisting of several subdetectors for the measurement of the momentum of charged particles (trackers), the energy measurement (calorimeters) and for muon detection. In Figure 2 a) an isometric view of the CDF detector is shown. The right-handed coordinate system used at CDF (Figure 2 b)) has its

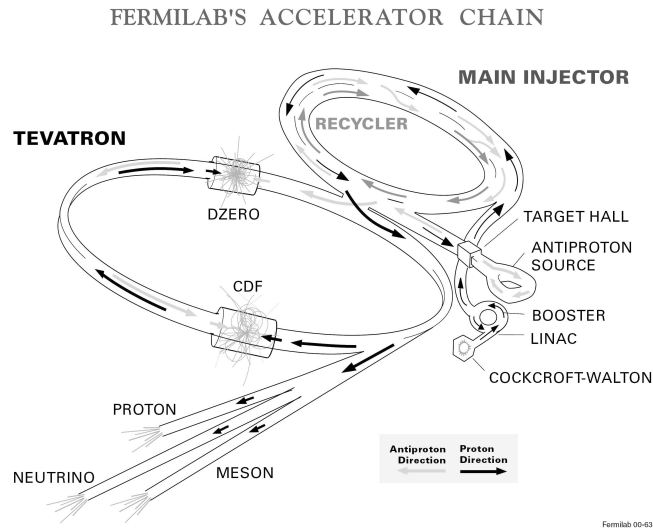


Abbildung 1: Schematic overview of the Tevatron accelerator with its two detectors $D\bar{0}$ and CDF and its preaccelerators.

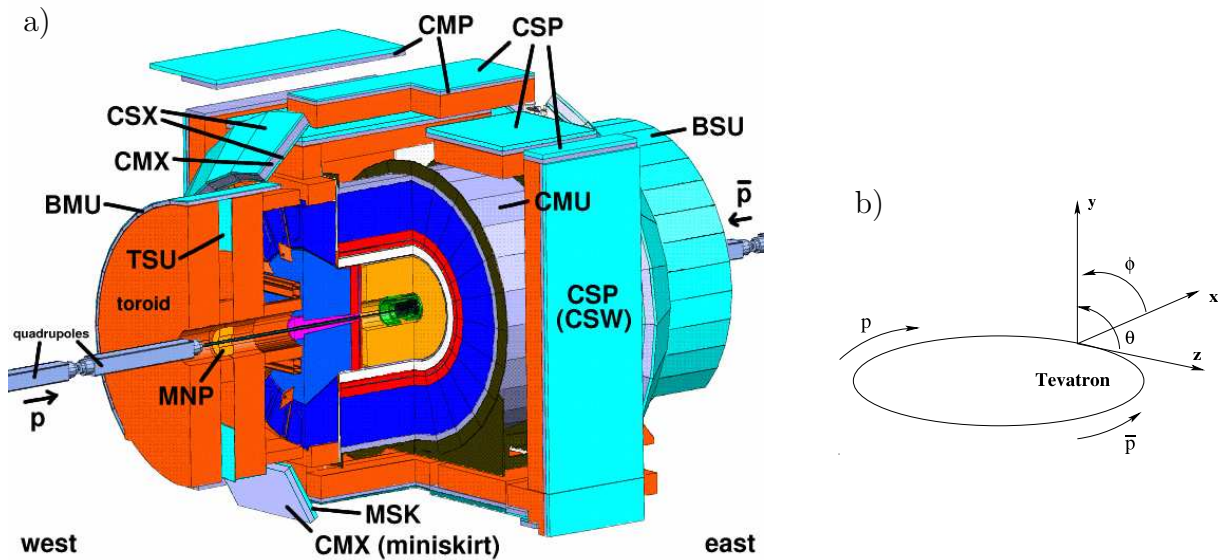


Abbildung 2: a) Isometric view of the CDF detector in Run II with the abbreviations of the different components of the muon system. The inner green and orange part represents the tracking system and the blue one the calorimeters. b) The coordinate system of the CDF II detector.

origin at the nominal interaction point. The z axis points in the proton beam direction. The x axis points away from the center of the Tevatron ring and the y -axis points perpendicular upwards. The azimuthal angle ϕ is measured with respect to the x axis in

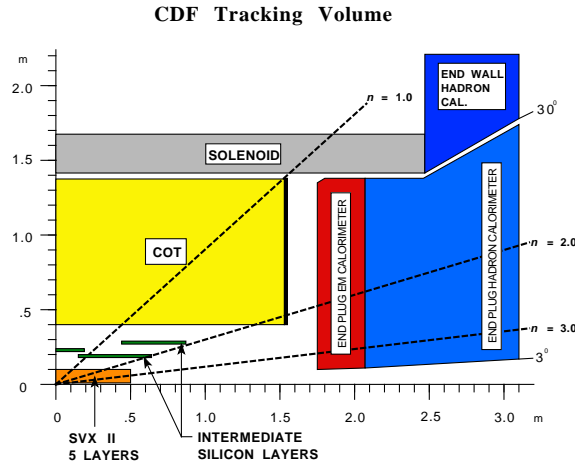


Abbildung 3: Longitudinal view of the CDF tracking system.

the xy plane. The polar angle θ is the angle with respect to the z -axis. Thus, the polar angle is $\theta = 0^\circ$ in proton direction and $\theta = 180^\circ$ in antiproton direction. The pseudorapidity is defined by $\eta = -\ln(\tan \frac{\theta}{2})$. A further often used quantity is the rapidity y , since differences in rapidity are Lorentz invariant. The rapidity is defined by $y = 1/2 \cdot \ln((E + p_z)/(E - p_z))$ and is equal to the pseudorapidity for massless particles. E is here the energy and p_z the z -component of the momentum of a particle. The detector components from the inner to the outer are:

- Tracking system:** The tracking system (Figure 3) consists of three major parts, a silicon based tracker, a drift chamber (COT = *Central Outer Tracker*), and a super-conducting solenoid. In the drift chamber the momentum and the direction of charged particles are measured via ionisation in gas, while in the silicon detectors the production of electron-hole pairs is exploited. The silicon system covers the region closest to the beam and extends from a radius of 1.35 cm to 28 cm. Seven layers of silicon sensors are arranged in a barrel-shaped geometry around the interaction point. An impact parameter resolution smaller than $< 30 \mu\text{m}$ is achieved in the xy plane for central high momentum tracks. Here, the impact parameter is the distance of closest approach of the track helix to the beam axis measured in the plane perpendicular to the beam. The second part of the tracking system is the COT, a 3.1 m long cylindrical drift chamber, to provide tracking at large radii in the region $|\eta| < 1.0$. The COT covers the radial range from 40 to 137 cm and a hit position resolution of approximately $140 \mu\text{m}$ and a momentum resolution of $\sigma(p_T)/p_T^2 = 0.0015 (GeV/c)^{-1}$ is obtained. The tracking system is surrounded by a super-conducting solenoid, 1.5 m in radius and 4.8 m in length, generating a 1.4 T magnetic field parallel to the beam axis.
- Calorimeter:** The solenoid and tracking volume is surrounded by the calorimeters, designed to measure the energy of particles and jets by fully absorbing all particles except muons and neutrinos. The calorimeter systems consists of an electromagnetic

and a hadronic part, both covering 2π in azimuth and the range in pseudorapidity from $\eta = -3.6$ to $\eta = 3.6$. The purpose of the electromagnetic calorimeters is to measure the energy of electromagnetic showers (caused by $e, \gamma, \pi^0 \rightarrow \gamma\gamma$), while the hadronic calorimeters are used to measure the energy of the hadronic showers (for example caused by π^\pm, K, n, p, \dots). The calorimeters are sampling calorimeters. The active medium is scintillator, the absorber is lead in the electromagnetic calorimeter and iron in the hadronic calorimeter. In this tutorial only electrons measured in the central part of the electromagnetic calorimeter are used. The coverage of this part is $|\eta| < 1.1$ and the energy resolution is $13.5\%/\sqrt{E} \oplus 2\%$.

- **Muon chambers:** Outside of the calorimeter the muon chambers are situated. Four systems of scintillators and drift tubes are used to detect muons at CDF: The *Central MUon Detection System* (CMU), the *Central Muon uPgrade* (CMP), the *Central Muon eXtension* (CMX) and the *Intermediate MUon system* (IMU). The CMU consists of four layers of drift chambers located outside the central hadronic calorimeter which acts as hadron absorber. It covers 84% of the solid angle for the pseudorapidity interval $|\eta| < 0.6$ and could be reached by muons with transverse momenta greater than 1.4 GeV/c. The CMP, which is located behind the CMU, consists of 0.6m of steel and additional four layers of drift chambers behind the steel. For $|\eta| < 0.6$ the CMP covers 63% of the solid angle while both systems have an overlap of 53% of the solid angle. The CMX covers the pseudorapidity range of $0.6 < |\eta| < 1.0$ to 71% of the solid angle and the IMU covers a range from $1.0 < |\eta| < 1.5$. In this tutorial only muons detected simultaneously in the CMU and CMP are used as well as muons detected in the CMX.

3 Physics of Top Quarks

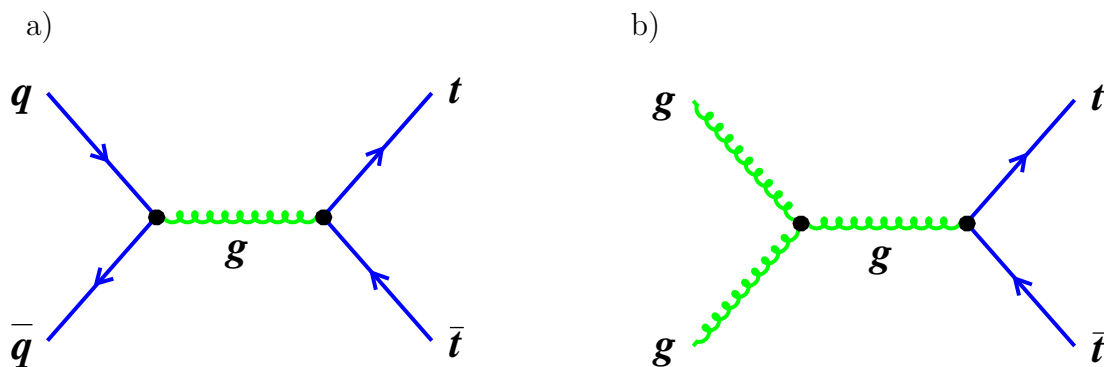


Abbildung 4: *Feynman diagrams of the top-antitop pair production. a) Quark-antiquark annihilation, b) gluon-gluon fusion.*

m_t [GeV/ c^2]	NLO σ [pb]
170	8.1 ± 0.7
175	6.9 ± 0.6
180	5.9 ± 0.5

Tabelle 1: $t\bar{t}$ cross section for different top-quark masses as predicted by the NLO calculations [1].

In $p\bar{p}$ collisions the dominant production mechanism of top quarks is pair production, while the electroweak production of single top quarks is much harder to detect due to very large backgrounds. Only recently, in 2009, single top-quark production was observed. In this tutorial we look only for $t\bar{t}$ -pair production.

At the Tevatron top-antitop pairs are produced via the strong interaction processes of quark-antiquark annihilation and gluon-gluon fusion, see Figure 4. In each case a parton (quark or gluon) of the proton interacts with a parton of the antiproton. At the Tevatron, quark-antiquark annihilation is the dominating production mechanism, contributing about 85% to the total cross section. while at the Large Hadron Collider (pp -collisions) at CERN gluon-gluon fusion will be the dominant process.

Calculations of the $t\bar{t}$ production cross section are performed at next-to-leading order (NLO) in perturbation theory. The predictions obtained by Moch and Uwer [1] are given in Table 1. Since top quarks are produced near the kinematic threshold at the Tevatron, the dependence of the cross section on the top-quark mass is substantial. The knowledge of the W -boson mass and top-quark mass constrains the Higgs mass. That is due to radiative corrections. Basically, virtual Higgs bosons are continuously emitted and reabsorbed by top quarks and W bosons, contributing to the observed mass of these particles. But if the top quark is found to be more massive, the Higgs also has to be more massive, while the opposite holds for W bosons.

The situation is illustrated in Figure 5. On the x axis is the top-quark mass, on the y axis the W -boson mass. Each point in this plane with a particular top-quark mass and W mass is related to a definite value of the as-of-yet unknown Higgs boson mass. The green band shows the region corresponding to allowed Higgs boson masses. The lines of equal mass range from 114 GeV, marking the experimental limit obtained from LEP2, up to 1000 GeV. The direct measurement of top-quark mass and W boson mass is shown as the blue ellipse. There is a 68% chance of the two true values of top and W masses to lie within the boundaries. The red dashed ellipse indicates the region favoured by the indirect measurements and LEP1 and SLD.

4 Signature of Top-Antitop Events

The top quark decays with a branching ratio of almost 100% into a b quark and W boson (see Figure 6 a)). Due to its large mass the lifetime of the top quark $\tau_t \propto 1/(G_F m_t^3)$ is

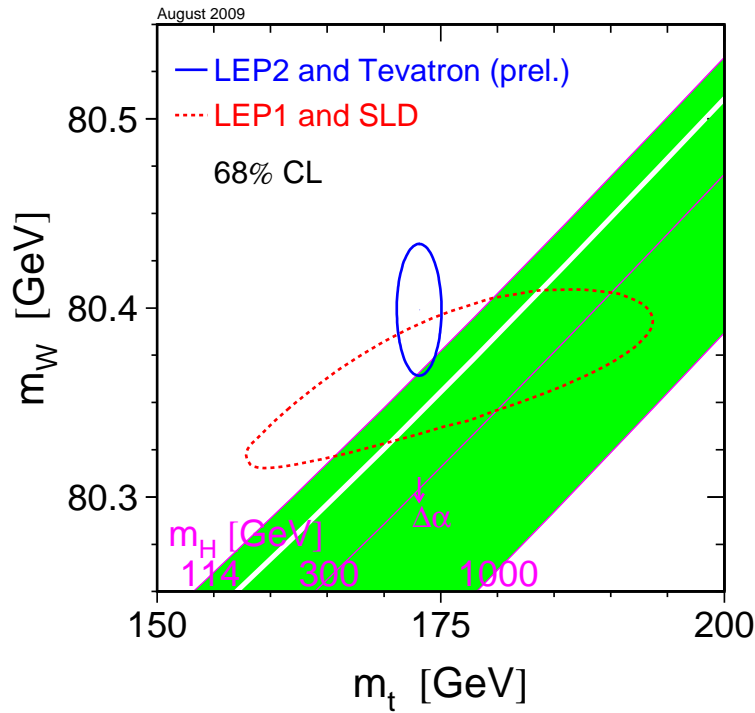
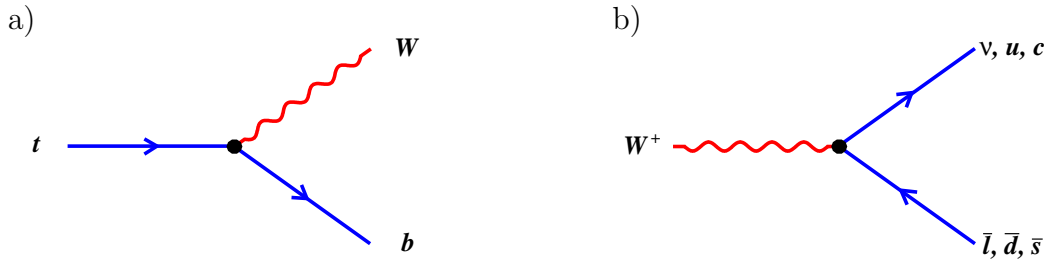


Abbildung 5: Constraining the Higgs boson mass. The W -boson mass is shown versus the top-quark mass.

rather small, $\tau_t \approx 5 \cdot 10^{-25}$ s, much smaller than the timescale of the hadronization process $\tau_{\text{hadron}} \sim 1 \text{ fm}/c \sim 3 \cdot 10^{-24}$ s. Thus, top quarks decay before they hadronize.

The W boson itself can decay semileptonically into a lepton and a neutrino or hadronically into quarks, which then hadronize into hadrons. The decay of the W boson is shown in Figure 6 b), while the branching ratios for the different decay modes of the W boson are summarized in Table 2. The two decay possibilities of the W boson lead to three different event topologies of $t\bar{t}$ events: dilepton events, lepton+jets events, and hadronic events. The different branching ratios of $t\bar{t}$ events, resulting from the combinations of the two W -boson decays, are presented in Table 3. A good compromise of high statistic samples with a large background contamination and low statistic samples with low background contamination is the selection of lepton+jets events, where one top quark decays semileptonically and where the second top quark decays hadronically. Top-quark events in the lepton+jets channel are thus characterized by a well isolated high-momentum lepton and substantial missing transverse momentum due to the undetected neutrino from the leptonic W decay, and a number of high-energy jets due to the hadronic W decay and two b -quark jets originating each from a top-quark decay. In Figure 7 an event display of

Abbildung 6: a) *Top decay*. b) *W-decay*.

W decay	Branching ratio
$e^+\nu_e$	$\sim 1/9 = 11.1\%$
$\mu^+\nu_\mu$	$\sim 1/9 = 11.1\%$
$\tau^+\nu_\tau$	$\sim 1/9 = 11.1\%$
$u\bar{d}$	$\sim 3/9 = 33.3\%$
$c\bar{s}$	$\sim 3/9 = 33.3\%$

Tabelle 2: Branching ratio for the W boson to decay into the various channels.

a $t\bar{t}$ -event candidate is shown.

In order to select $t\bar{t}$ events only electrons and muons are considered as charged leptons, no taus, since the signature of taus in the detector is not as clear as of electrons or muons. Isolated electrons and muons with a transverse momentum p_T above 20 GeV are required. Isolated means, that in a certain cone around the charged lepton there is almost no energy deposition from further particles in the calorimeter. To reduce background from Z -boson events only events with exactly one high-momentum lepton are accepted. A further reduction of Z -boson events is achieved, by removing events where the selected charged lepton and a second object form an invariant mass within a window around the Z mass. Jets are reconstructed using the cone algorithm, where all particles within a cone of a given size are assigned to one jet. Jets are called high energetic jets, when the transverse energy is $E_T = E \cdot \sin \theta > 15$ GeV and $|\eta| < 2.0$. The preselected sample used in this tutorial was obtained by requiring at least one high energetic jet. Furthermore, a missing transverse energy of ≥ 20 GeV is required.

The most relevant background process of $t\bar{t}$ events is W -boson plus jets production. These jets can be of light flavor (u , d , or s) or originate from heavy quarks (c and b). Light flavor jets are dominating, while heavy flavor jets make up only a few percent of jets associated to a W boson. A further source of background events are QCD processes where one jet fakes an electron or where a muon coming from a b or c quark decay is measured as isolated.

Due to the large top-quark mass the decay products of top-quark decay carry large

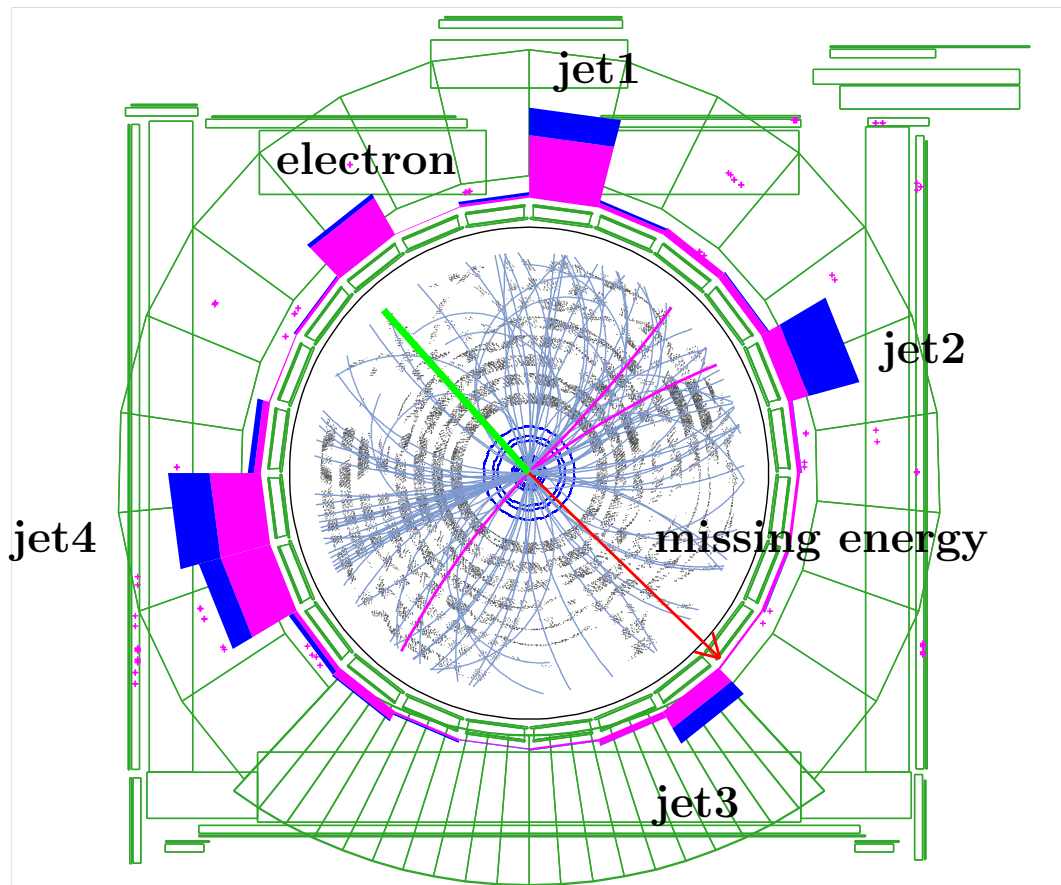


Abbildung 7: Event display of a $t\bar{t}$ candidate with four jets. The energy of the electromagnetic calorimeter towers are drawn magenta, the energy of the hadronic calorimeter towers are drawn blue. The size of the cluster is proportional to the measured energy. The red arrow represents the direction of the missing energy. The inner part of the picture represents the tracking system. The gray points are hits in the COF, the blue points of the inner most rings are hits of the silicon vertex detector. The green line, an isolated track pointing to an energy deposition in the electromagnetic calorimeter represents the electron.

W_1 decay	W_2 decay	Branching ratio
Dilepton channel		
$e^+\nu_e$	$e^+\nu_e$	$\sim 1/81 = 1.2\%$
$e^+\nu_e$	$\mu^+\nu_\mu$	$\sim 2/81 = 2.4\%$
$e^+\nu_e$	$\tau^+\nu_\tau$	$\sim 2/81 = 2.4\%$
$\mu^+\nu_\mu$	$\mu^+\nu_\mu$	$\sim 1/81 = 1.2\%$
$\mu^+\nu_\mu$	$\tau^+\nu_\tau$	$\sim 2/81 = 2.4\%$
$\tau^+\nu_\tau$	$\tau^+\nu_\tau$	$\sim 1/81 = 1.2\%$
Hadronic channel		
$q\bar{q}$	$q\bar{q}$	$\sim 36/81 = 44.4\%$
Lepton + jets channel		
$e^+\nu_e$	$q\bar{q}$	$\sim 12/81 = 14.8\%$
$\mu^+\nu_\mu$	$q\bar{q}$	$\sim 12/81 = 14.8\%$
$\tau^+\nu_\tau$	$q\bar{q}$	$\sim 12/81 = 14.8\%$

Table 3: Branching ratio of $t\bar{t}$ events for the two W -boson to decay into the various combinations.

transverse momentum. A feature which is not present to the same extent in background processes. Therefore, the scalar sum of the transverse momenta in an event is a powerful discriminant between $t\bar{t}$ events on one hand and W +jets events on the other hand. Traditionally, this variable is called H_T , since it exerts *Herculean* power in suppressing background. In the tutorial we will use this variable to measure the $t\bar{t}$ content of the sample of candidate events. Since the shape of the H_T variable is quite similar the different background processes, only the W -boson plus light jet background is considered.

b-jet identification In $t\bar{t}$ events two b -quark jets should exist. For the identification of b -jets, thus jets, which contain one or more b hadrons, the long lifetime of the b hadrons is exploited. The travel distance of a b hadron from its production vertex to its decay vertex is large enough to be resolved using the silicon tracker. b -jets coming from top-quark decays at the Tevatron have an average p_T of about 65 GeV, while the lifetime of a b hadron is about, 1.5 picoseconds. Therefore, the average distance traveled in the lab frame before decaying is approximately 7.5 millimeters.

The b -tagging algorithm used by CDF, looks for tracks in each jet that are displaced from the primary vertex. The impact parameter has to be $|d_0| \leq 0.3$ cm (see figure 8). If there are at least two of these displaced tracks in the jet the tagging algorithm attempts to fit these tracks to a common vertex. As a final step the tagging algorithm computes the distance between the primary and secondary vertex in the $r - \phi$ plane, L_{xy} (fig. 8). A cut on the significance L_{xy}/σ_{xy} of the displacement of ≥ 7.5 is required for so called b -tagged jets. Requiring that at least one selected jet is tagged as b -jet leads to a strong background reduction.

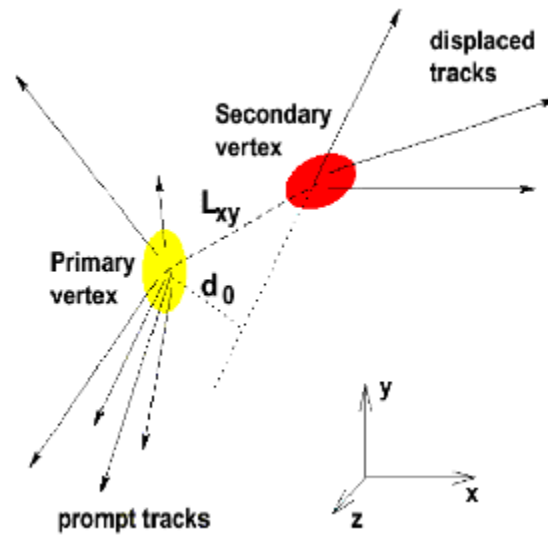


Abbildung 8: *General principle of b-tagging. The impact parameter d_0 and the decay length L_{xy} are sketched.*

For further reading on top-quark physics we recommend the review article [2].

Literatur

- [1] S. Moch and P. Uwer, Nuclear Phys. Proc. Suppl. 183 (2008) 75.
- [2] J.R. Incandela, A. Quadt, W. Wagner, D. Wicke, Prog. Part. Nucl. Phys. 63 (2009) 239 – 292.